



# Development of Magnetic Solid Phase Micro-Extraction (MSPE) Method for the Extraction and Preconcentration of the Selected $\beta$ -Blockers in the Environmental Wastewaters

Ngwako Joseas Waleng<sup>1,2</sup> · Shirley Kholofelo Selahle<sup>1,2</sup> · Anele Mpupa<sup>1,2</sup> · Yongjun Zhang<sup>3</sup> · Philiswa Nosizo Nomngongo<sup>1,2,4</sup>

Received: 29 November 2023 / Accepted: 31 March 2024

© The Author(s) 2024

## Abstract

Emerging organic pollutants have always been the greatest environmental concern due to their ubiquity and distinguished adverse effects. These are mostly water-borne pollutants flagged as endocrine disruptors and can greatly inconvenience the ecosystem. Among others,  $\beta$ -blockers have also been detected in the environment at various concentrations that threaten the well-being of humans and animals. In this work,  $\text{NH}_2$ -MIL-101(Cr) doped magnetic nanoparticles nanocomposite was successfully synthesised and characterised using analytical techniques such as X-ray diffraction spectroscopy (XRD), scanning electron microscopy (SEM), Fourier transform infrared spectroscopy (FTIR), Brunauer-Emmett-Teller (BET) and transmission electron microscopy (TEM). The  $\text{Fe}_3\text{O}_4@ \text{NH}_2$ -MIL-101(Cr) was then used as an adsorbent to extract the selected  $\beta$ -blockers in the environmental wastewater. The selected  $\beta$ -blockers were quantified using a high-performance liquid chromatography-diode array detector (HPLC-DAD). Parameters affecting the extraction were screened and optimised using fractional factorial design (FFD) and central composite design (CCD), respectively. Under optimum conditions, the LODs were 0.057 and 0.065  $\mu\text{g L}^{-1}$ , and LOQs were 0.19 and 0.22  $\mu\text{g L}^{-1}$  for acebutolol (ACE) and metoprolol (MET), respectively. The calibration curve exhibited the linearity range of 0.2–1200  $\mu\text{g L}^{-1}$  with correlation coefficients of 0.9987 and 0.9968 for ACE and MET, respectively. Repeatability studies demonstrated the %RSD of 0.63 and 0.74% for MET and ACE. At the same time, reproducibility studies displayed the %RSD of 1.057 and 1.178% for MET and ACE, respectively. Spike recovery experiments were carried out to assess the performance of MSPE in real samples, and over 88% of both analytes were recovered. This indicated that the MSPE method could enrich various organic pollutants from different environmental matrices.

**Keywords** Solid-phase Extraction · Metal Organic Frameworks ·  $\beta$ -blockers · Central Composite Design

✉ Philiswa Nosizo Nomngongo  
pnnomngongo@uj.ac.za

<sup>1</sup> Department of Chemical Sciences, University of Johannesburg, Doornfontein Campus, 2028 Johannesburg P. O. Box 17011, South Africa

<sup>2</sup> Department of Science and Innovation-National Research Foundation South African Research Chair Initiative (DSI-NRF SARChI) in Nanotechnology for Water, University of Johannesburg, 2028 Doornfontein, South Africa

<sup>3</sup> School of Environmental Science and Engineering, Nanjing Tech University, Puzhu Nan Lu 30, 211800 Nanjing, PR China

<sup>4</sup> DSI/Mintek Nanotechnology Innovation Centre, University of Johannesburg, 2028 Doornfontein, South Africa

## 1 Introduction

Over the past few years, many pharmaceuticals have been released into the ecosystem through distinguished mechanisms. The emergence of new diseases and the need to mitigate global health challenges faced by humans and animals have led to increased production of new pharmaceuticals [1, 2].  $\beta$ -blockers are a class of pharmaceuticals frequently detected in the environment at concentrations ranging from  $\text{ng L}^{-1}$  to  $\mu\text{g L}^{-1}$ . Intact or metabolised  $\beta$ -blockers escape through wastewater treatment plants (WWTPs) due to their high solubility in water, found in sewage effluents and surface and ground waters [3]. The ubiquitousness of  $\beta$ -blockers in the environment is associated with their

extremely adverse effects on aquatic and terrestrial organisms, including humans. These negative effects include reduced testosterone levels, disruption of the endocrine system, and sexual dysfunction. The health impacts result from the continuous consumption of  $\beta$ -blockers with amounts exceeding maximum allowable daily limits of  $\mu\text{g}\text{-ng}/\text{dm}^3$  [4–8]. Therefore, a great scope of research is to devise effective methods for eliminating these recalcitrant pollutants. Removal methods including adsorption, photodegradation, membrane filtration among others have been greatly considered for the elimination of these recalcitrant  $\beta$ -blockers [9–11]. However, these compounds exist at the lowest concentrations due to their extreme dilution when they enter the environmental water systems, making it impracticable for their analytical detection even when using advanced sensitive analytical techniques [12, 13]. Therefore, the preconcentration step is necessary.

Various sample preparation methods have been adopted to preconcentrate numerous environmental pollutants. Among others, solid-phase extraction (SPE) and liquid-liquid extraction (LLE) have been widely used as traditional sample preparation methods [14, 15]. However, these methods are time-consuming, laborious, costly and environmentally unfriendly. Additionally, LLE uses large volumes of harmful organic solvents [16, 17]. Therefore, the attention has been shifted to using miniaturised sample preparation methods such as liquid-phase microextraction (LPME) [18], solid-phase microextraction (SPME) [19], dispersive liquid-phase microextraction (*d*-LPME) [20] and dispersive solid phase microextraction (*d*-SPME) [21], among others. These methods can preconcentrate the analytes of interest and ultimately clean up the matrix with enhanced efficacy [22, 23].

$\beta$ -blockers can be quantified by a wide range of analytical techniques, including high pressure liquid chromatography coupled to various detectors (HPLC) [19, 24], gas chromatography-mass spectrometry (GC-MS) [25], micellar electrokinetic chromatography (MEKC) [26], electrochemical detection [27] and capillary zone electrophoresis (CZE) [28]. Among these techniques, HPLC is currently considered for the quantification of the majority of polar non-volatile organic pollutants owing to its greater sensitivity, selectivity and separation efficiency [29].

This work used magnetic solid phase extraction (MSPE) as a sample preparation method for the preconcentration of the selected  $\beta$ -blockers. The choice of this method is associated with intriguing features, including the use of a small mass of adsorbents (MA), small non-toxic organic solvent volumes, reduced extraction times, easy adsorbent recovery and cost-effective operation [30]. The chosen preconcentration method requires the incorporation of a suitable adsorbent to enhance the selectivity of target analytes and subsequently improve the extraction performance. Metal-organic

frameworks (MOFs) have been successfully used in various applications, including gas storage, catalysis, gas sensors and adsorption [29]. MOFs are porous crystalline materials of metal ions or clusters coordinated to organic ligands. The key features of MOFs include large specific surface area, physical stability, large pore volumes and tunable structural moieties that encourage interactions with target analytes [31]. Recently, MOFs prevailed as promising candidates as adsorbents in environmental wastewater remediation owing to their fascinating features stated above [32]. Amino-based MIL-101(Cr) ( $\text{NH}_2$ -MIL-101(Cr)) has been largely used as an adsorbent for the adsorption of various pollutants but was never used before as a solid-phase for the extraction and preconcentration of the selected  $\beta$ -blockers (acebutolol (ACE) and metoprolol (MET)). The motivation behind the choice of these two  $\beta$ -blockers includes: (i) metoprolol is regarded as the most used antihypertensive drug and it more likely to be found in the environment at concentrations posing serious health concerns, (ii) acebutolol is used mostly on people having asthmatic attacks or with obstructive pulmonary disease and therefore, its environmental ubiquity is inevitable [33]. Hence, the current work exploited the fascinating features of  $\text{NH}_2$ -MIL-101(Cr) to be used as an adsorbent to extract and preconcentrate ACE and MET from environmental water samples. The main beneficial feature about the use of  $\text{NH}_2$ -MIL-101(Cr) is that, Cr(III) is considered as an environmentally beneficial micronutrient which is essential for organisms.

Furthermore, Cr(III) can form complexes or adsorb onto organic and inorganic substances under neutral and basic conditions [32]. However, recovering  $\text{NH}_2$ -MIL-101(Cr) from aqueous solutions after the extraction process is tedious and time-consuming; thus, magnetic nanoparticles ( $\text{Fe}_3\text{O}_4$ ) were incorporated to facilitate the sorbent recovery using an external magnet. Furthermore,  $\text{Fe}_3\text{O}_4$  nanoparticles contribute to some additional active adsorption sites, which ultimately improved the performance of the method [32].

Herein, we report the development of the MSPE method coupled with HPLC for the extraction and preconcentration of the selected  $\beta$ -blockers using  $\text{Fe}_3\text{O}_4@ \text{NH}_2$ -MIL-101(Cr) nanocomposite as a solid support.  $\text{Fe}_3\text{O}_4@ \text{NH}_2$ -MIL-101(Cr) was synthesised based on the in-situ chemical co-precipitation method proposed by [34]. A series of characterisation techniques were employed to confirm the synthesised materials. Various factors affecting the method, such as extraction time (ET), mass of adsorbent (MA), desorption time (DT), eluent volume (EV) and sample pH, were also investigated. This work provided advanced insights into MOFs as adsorbents for sample pretreatment methods and further demonstrated the promising applicability of MOFs as efficient adsorbents.

## 2 Experimental

### 2.1 Materials

Sodium hydroxide, hydrochloric acid (37%), iron (II) chloride tetrahydrate, iron (III) chloride hexahydrate, chromium (III) nitrate nonahydrate, 2-aminoterephthalic acid, acetone, acetonitrile (HPLC grade), ethanol, dimethylformamide (DMF), 5,5-dimethyl-1-pyrroline N-oxide (DMPO), hydrogen peroxide and ammonium solution (25%), were purchased from Sigma Aldrich (St. Louis, MO, USA). Metoprolol (MET) and Acebutolol (ACE) analytical standards were also purchased from Sigma Aldrich. A 200 mg/L stock solution of MET and ACE was prepared in methanol and kept in the refrigerator at 4 °C. Working solutions were prepared by diluting the stock solution with ultrapure water obtained from Direct-Q® 3UV-R purifier system (Millipore, Merck, Germany) and ultrapure water was in all experiments.

### 2.2 Synthesis of Fe<sub>3</sub>O<sub>4</sub> Nanoparticles and NH<sub>2</sub>-MIL-101(Cr)

Synthesis of Fe<sub>3</sub>O<sub>4</sub> followed the co-precipitation procedure reported in the literature [14]. The synthesis of NH<sub>2</sub>-MIL-101(Cr) was according to method reported elsewhere [35]. In a typical hydrothermal procedure, 3.2 g chromium nitrate nonahydrate and 1.44 g 2-aminoterephthalic acid were added into 60 mL solution containing 0.8 g sodium hydroxide. The mixture was then stirred for 30 min at room temperature to form a homogeneous solution and transferred into a 100 mL Teflon-lined stainless steel autoclave. The autoclave was heated at 150 °C for 12 h. After cooling to room temperature for over 6 h, the suspension was separated via centrifugation and repeatedly washed with DMF, Ethanol and ultrapure water. The resulting product was dried at 100 °C overnight.

### 2.3 Synthesis of Fe<sub>3</sub>O<sub>4</sub>@NH<sub>2</sub>-MIL-101(Cr)

Fe<sub>3</sub>O<sub>4</sub>@NH<sub>2</sub>-MIL-101(Cr) was synthesised using the chemical co-precipitation method reported in the literature [34]. Briefly, 1 g of NH<sub>2</sub>-MIL-101(Cr) was added into 150 mL ultrapure water containing 3.02 g Fe (III) and 2.01 g Fe(II). Subsequently, 15 mL of ammonium solution was added to the solution while stirring for 30 min at room temperature to form a black suspension. The precipitates were collected by magnetic decantation and repeatedly washed with acetone and ultrapure water. The product was then dried at 60 °C for further use.

### 2.4 Instrumentation

The synthesised materials were characterised using the following analytical techniques: Infrared spectra were recorded on Perkin Elmer Spectrum 100 Fourier Transform infrared spectrophotometer (Waltham, MA, USA) using the KBr pellet technique. Surface area and pore size distribution of the materials were obtained using Brunauer-Emmet-Teller by nitrogen adsorption-desorption technique in a Micrometric ASAP 2020, and all the gases utilised for analytical procedures were instrument grade. Crystallinity and X-ray diffraction patterns were determined by Powdered X-ray diffraction (X'Pert Phillips) with CuK $\alpha$  radiation at 0.1540 nm. The internal morphology was observed using transmission electron microscopy (TEM, JEM-200X, JEOL, Japan). The point of zero charge of the material was obtained using the pH drift method.

Chromatographic analysis was conducted on an Agilent 1200 Infinity series coupled to a diode array detector (Agilent Technologies, Waldbronn, Germany). An Agilent Zorbax Eclipse Plus C18 column (3.5  $\mu$ m x 150 mm x 4.6 mm) (Agilent, Newport, CA, USA) was operated at a column temperature of 25 °C. The isocratic elution mode was used with a mobile phase composition of 80:20 v/v 10mM H<sub>3</sub>PO<sub>4</sub> to acetonitrile. A flow rate of 0.800 mL/min was used throughout the analysis, and a run time of 7 min for each sample was selected for the method. The chromatograms were recorded at 220 nm for both analytes.

### 2.5 Adsorption Isotherms and Capacity

The adsorption capacity of the nanocomposite for both ACE and MET was obtained by conducting adsorption isotherms studies. The adsorption isotherms studies were conducted to get insight into the surface chemistry of the adsorbent and the adsorption behaviour. In a typical procedure, 60 mg of Fe<sub>3</sub>O<sub>4</sub>@NH<sub>2</sub>-MIL-101(Cr) was placed in 300 mL Erlenmeyer flasks containing 250 samples with varying concentrations (2–8 mg L<sup>-1</sup>). The samples were then sonicated for 30 min at ambient temperature. The solution pH was maintained at 9. The resulting supernatants were then magnetically separated and filtered into the HPLC vials. The formula below was used to calculate the adsorption capacity ((Q<sub>e</sub> (mg g<sup>-1</sup>)).

$$Q_e = \frac{(C_0 - C_e)V}{W} \quad (1)$$

Where C<sub>0</sub> (mg L<sup>-1</sup>) and C<sub>e</sub> (mg L<sup>-1</sup>) represent the initial and final concentrations; Q<sub>e</sub> (mg g<sup>-1</sup>) represent adsorption capacity, V (mL) represents the sample volume, and W (mg) represents the mass of adsorbent. The adsorption mechanism

was further understood by correlating the experimental data to different models such as Langmuir, Freundlich, Dubunin-Radushkevich (D-R), and Sips [36].

## 2.6 Sample Collection

Wastewater samples used in this work were collected from Daspoort wastewater treatment plant (WWTP) and Pienaars river water situated at Pretoria, Gauteng Province, South Africa. This treatment plant uses the activated sludge system to treat the domestic and industrial wastewaters which are 95% and 5% of treated materials, respectively. The collected influent, effluent and river water samples were then collected into the amber bottles and stored in the fridge at 4 °C. Before every analysis, the samples were filtered off the large particulates using 0.45 µm syringe filters.

## 2.7 Magnetic Solid-Phase Extraction Procedure (MSPE)

The preparation of the  $\beta$ -blockers model solution of 300 µg L<sup>-1</sup> was carried out by diluting a stock solution of 10 mg L<sup>-1</sup>. The extraction and preconcentration procedure was carried out as illustrated on the schematic diagram in Fig. 1. Firstly, an amount (10–60 mg) of Fe<sub>3</sub>O<sub>4</sub>@NH<sub>2</sub>-MIL-101(Cr) adsorbent was placed into the amber bottle containing a certain

volume of the 300 µg L<sup>-1</sup> ACE and MET. The extraction of the analytes from the aqueous solution onto the adsorbent was executed by ultrasonication for about 5–20 min. Then the resulting supernatant was magnetically decanted, and about 100–1000 µL of the eluting solvent (acetonitrile) was added onto the supernatant-free adsorbent containing analytes. The mixture was then ultrasonicated for about 5–15 min for desorption of the analytes into the eluent solvent. The aqueous solution was magnetically separated from the adsorbent and filtered through 0.22 µm syringe filters into amber vials, and the analytes were subsequently quantified using HPLC-DAD. The predetermined influential factors affecting the preconcentration method were screened and optimised using fractional factorial design (FFD) and central composite design (CCD), respectively. Table 1 shows factors along with their levels used in FFD.

## 2.8 Reusability Studies

Adsorption-desorption experiments were conducted to evaluate the regenerability and reusability of Fe<sub>3</sub>O<sub>4</sub>@NH<sub>2</sub>-MIL-101(Cr) nanocomposite. The extraction and preconcentration procedures were performed using optimised parameters viz.; 70.1 mg, 10 min, 5 min, 1000 µL and 10.21 for MA, ET, DT, EV and pH, respectively. In a typical procedure, the spent adsorbent was treated with

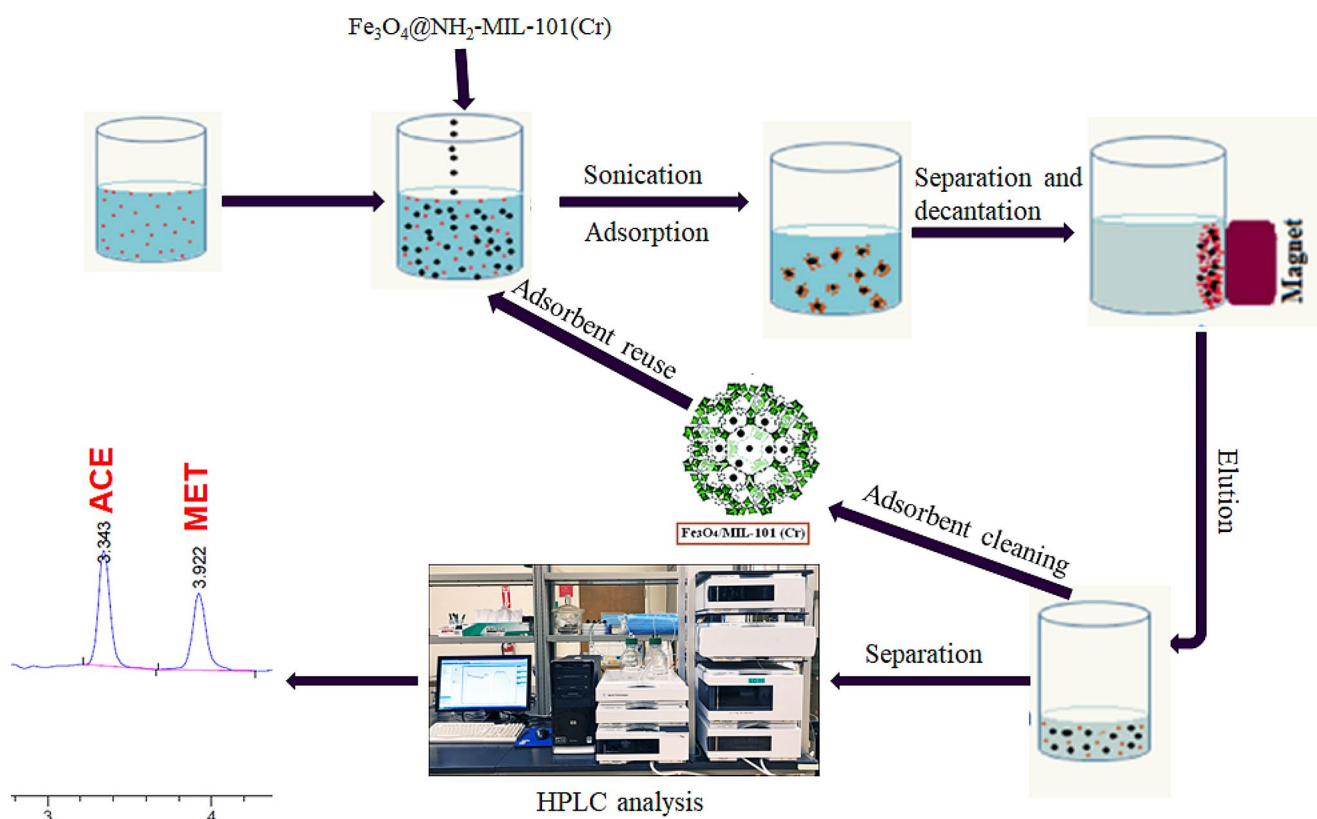


Fig. 1 Summary of the MSPE procedure and adsorbent reusability

**Table 1** Factors with corresponding levels used in CCD for MSPE optimisation

Variables	Low level (-1)	Central point (0)	High level (+1)
Mass of adsorbent (mg)	10	35	60
Extraction time (min)	5	12.5	20
Desorption time (min)	5	10	15
Eluent volume ( $\mu\text{L}$ )	100	550	1000
pH	3	6	9

ultrapure water and ethanol, then dried in the oven at 70 °C for 1 h. The regenerated adsorbent was then applied in the 2nd cycle of extraction. The process was repeatedly conducted until the adsorption capacity of the adsorbent performance was remarkably reduced.

## 2.9 Method Validation

To evaluate the efficacy and the validity of the proposed sample preparation analytical procedure, validation step is inevitable. In this work, method validation was conducted based on the International Guidelines and the validation included the evaluation of the analytical parameters including: limits of detection and quantification (LOD and LOQ), linearity, specificity, precision (intra-day and inter-day studies) and accuracy (efficiency of the method in real water samples). Based on International Union of Pure and Applied Chemistry (IUPAC), the LOD and LOQ are defined as the minimum levels of the analytes that can give responses equal to 3.3 SD/m and 10 SD/m, respectively, where m represents the slope of the calibration curve and SD stands for standard deviation [14]. The calibration curve linearity parameter is obtained by assessing the correlation of determination ( $R^2$ ) when the concentration of the analytes within the prepared standard solution is plotted as a function of the detector response of the HPLC instrument. Specificity refers to the ability of the method to honestly maintain the extraction of the specified analytes regardless of the presence of other matrix components. Accuracy is the proximity of the measured values to the true value when measurements are repeatedly conducted. Precision is the proximity of the measured values to each other and it was conducted in two ways in the current work: (i) The first precision test was repeatability which involved performing the experiments on the same day using the same operating parameters, (ii) Second precision test was reproducibility which involved performing experiments at different days using different operating parameters. To evaluate the effect of the matrix on the performance of the method, calibration curves prior and after extraction were obtained and the matrix effect percentage (ME%) was calculated using the formula below:

$$\%ME = \frac{\text{Slope of the matrix} - \text{slope of the solvent}}{\text{slope of the solvent}} \times 100 \quad (2)$$

## 2.10 Application of the Preconcentration Method to Real Samples (Accuracy)

The MSPE method was then applied to real samples to extract and preconcentrate the selected  $\beta$ -blockers using the optimum conditions. Figure 1 summarises the method for extracting and preconcentrating the selected  $\beta$ -blockers in real samples.

## 3 Results and Discussion

### 3.1 Characterisation of the Materials

#### 3.1.1 Fourier Transform Infrared Spectroscopy

Functional groups on  $\text{Fe}_3\text{O}_4$ ,  $\text{NH}_2\text{-MIL-101(Cr)}$  and  $\text{Fe}_3\text{O}_4@\text{NH}_2\text{-MIL-101(Cr)}$  were verified on FTIR spectroscopy. The FTIR spectra for the materials are shown in Fig. 2. From the FTIR spectrum of  $\text{Fe}_3\text{O}_4$ , a highly intense peak at  $548\text{ cm}^{-1}$  corresponding to the stretching vibration of Fe-O, indicating the successful synthesis of magnetic nanoparticles, was observed. Moreover, the intensive peaks appearing at  $1481$  and  $1640\text{ cm}^{-1}$  belong to the C-O and C=O of carbon dioxide from the air [37]. In the spectrum of  $\text{NH}_2\text{-MIL-101(Cr)}$ , noticeable peaks were observed at  $3084$  and  $3467\text{ cm}^{-1}$ , indicating the symmetric and asymmetric stretching vibrations of primary amine groups. The absorption bands at  $1396$  and  $1622\text{ cm}^{-1}$  are characteristic of the symmetrical and asymmetrical stretching vibrations of carboxylate ligands of the deprotonated terephthalate ligands [38, 39]. This confirms the presence of double carboxylic acid groups on the structure of  $\text{NH}_2\text{-MIL-101(Cr)}$ . Furthermore, benzene C-H vibrations bands were exhibited at  $1017\text{ cm}^{-1}$  and  $748\text{ cm}^{-1}$  [40]. The peak at around  $666\text{ cm}^{-1}$  indicates the Cr-O vibration band, confirming the successful synthesis of  $\text{NH}_2\text{-MIL-101(Cr)}$  [34]. In the nanocomposite spectrum, an intense peak at  $548\text{ cm}^{-1}$  was attributed to Fe-O tensile vibration, confirming the successful doping of magnetic nanoparticles on  $\text{NH}_2\text{-MIL-101(Cr)}$ . The successful synthesis of  $\text{Fe}_3\text{O}_4@\text{NH}_2\text{-MIL-101(Cr)}$  was further accounted for by the presence of both Cr and Fe atoms in the nanocomposite.

#### 3.1.2 Brunauer–Emmett–Teller

Table 2 shows BET results of  $\text{Fe}_3\text{O}_4@\text{NH}_2\text{-MIL-101(Cr)}$ . This technique was employed to establish the surface properties of the materials using the  $\text{N}_2$  adsorption-desorption

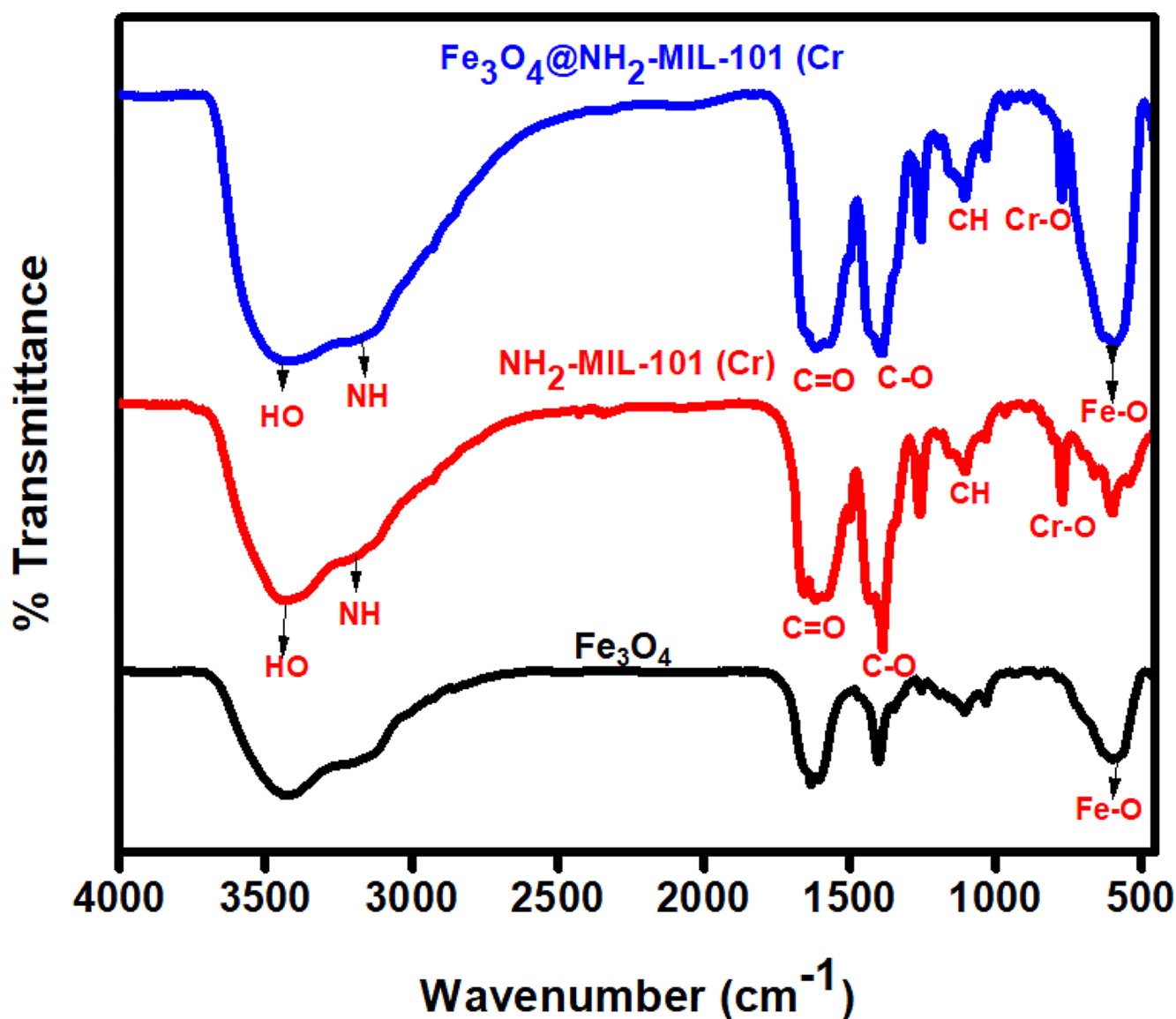


Fig. 2 FTIR spectra of  $\text{Fe}_3\text{O}_4$ ,  $NH_2\text{-MIL-101(Cr)}$  and  $\text{Fe}_3\text{O}_4@NH_2\text{-MIL-101(Cr)}$

**Table 2** BET surface area, pore volumes and pore sizes of  $\text{Fe}_3\text{O}_4$ ,  $NH_2\text{-MIL-101(Cr)}$  and  $\text{Fe}_3\text{O}_4@NH_2\text{-MIL-101(Cr)}$

Materials	Surface area ( $\text{m}^2 \text{g}^{-1}$ )	Pore volume ( $\text{cm}^3 \text{g}^{-1}$ )	Pore size (nm)
$\text{Fe}_3\text{O}_4$	190.6	0.28	1.96
$NH_2\text{-MIL-101 (Cr)}$	2553.74	0.51	1.45
$\text{Fe}_3\text{O}_4@NH_2\text{-MIL-101 (Cr)}$	1982.67	0.33	2.34

technique. The  $N_2$  adsorption-desorption isotherms of  $\text{Fe}_3\text{O}_4$ ,  $NH_2\text{-MIL-101(Cr)}$  and  $\text{Fe}_3\text{O}_4@NH_2\text{-MIL-101(Cr)}$  shown in (Online Resource 5) were obtained at 77 K. As shown in Online Resource 5, the nanocomposite exhibited type IV isotherm, indicating the mesoporous nature of the internal structure. Specific surface area, pore size and pore volume for  $\text{Fe}_3\text{O}_4$ ,  $NH_2\text{-MIL-101(Cr)}$  and

$\text{Fe}_3\text{O}_4@NH_2\text{-MIL-101(Cr)}$  are listed in Table 2. After doping  $NH_2\text{-MIL-101 (Cr)}$  with  $\text{Fe}_3\text{O}_4$  nanoparticles, specific surface area and pore volume dropped significantly, showing that  $\text{Fe}_3\text{O}_4$  partially occupied active moieties on  $NH_2\text{-MIL-101(Cr)}$ . The increase in pore size of the nanocomposite was a result of the internal pore strain resulting from the incorporation of the  $\text{Fe}_3\text{O}_4$  nanoparticles. Nonetheless, the reduced specific surface area was sufficient for the efficient extraction of the selected  $\beta$ -blockers.

### 3.1.3 X-Ray Diffraction Spectroscopy

The structural phase and composition of  $\text{Fe}_3\text{O}_4$ ,  $NH_2\text{-MIL-101(Cr)}$  and  $\text{Fe}_3\text{O}_4@NH_2\text{-MIL-101(Cr)}$  were evaluated on XRD spectroscopy and the results are shown in

Fig. 3. The spectrum of  $\text{Fe}_3\text{O}_4$  (Fig. 3(a)) revealed the crystalline peaks which were in accordance with the XRD pattern reported in the previous studies [41]. In the XRD spectrum of  $\text{NH}_2\text{-MIL-101(Cr)}$  (Fig. 3(b)), salient crystalline patterns were observed at  $2\theta$  angles of  $10.6^\circ$ ,  $17.9^\circ$ ,  $25.6^\circ$ ,  $34.6^\circ$  and  $43.7^\circ$  which were similar with those previously [42]. In XRD spectrum of the nanocomposite (Fig. 3(c)), the main diffraction peaks of  $\text{Fe}_3\text{O}_4$  were still observed  $2\theta$  angle of  $30.2^\circ$ ,  $37.7^\circ$ ,  $41.5^\circ$ ,  $54.5^\circ$ ,  $58.7^\circ$  and  $65.3^\circ$ , which matched (220), (311), (400), (422), (511) and (440) planes of typical crystalline structure of  $\text{Fe}_3\text{O}_4$  (JCPDS file 19-0629). However, the observed diffraction peaks of  $\text{NH}_2\text{-MIL-101(Cr)}$  at  $2\theta$  angles of  $10.6^\circ$ ,  $17.9^\circ$ ,  $25.6^\circ$  have merged into a broad peak appearing at  $2\theta$  range from  $10\text{-}27.1^\circ$ , indicating successful synthesis of the nanocomposite. The disappearance of peaks at  $2\theta$  around  $34.6^\circ$  and  $43.7^\circ$  in comparison with  $\text{NH}_2\text{-MIL-101(Cr)}$  was clear evidence for the characteristic growth of crystal planes and decrescent in crystallite size [43]. The appearance of the predominating main peaks of  $\text{Fe}_3\text{O}_4$  on the XRD spectrum of the nanocomposite indicated that  $\text{Fe}_3\text{O}_4$  nanoparticles fairly distributed on the surface of  $\text{Fe}_3\text{O}_4@\text{NH}_2\text{-MIL-101(Cr)}$ . This was further confirmed by TEM results (Fig. 4).

### 3.1.4 Transmission Electron Microscope

The internal structures and micro-compositions of  $\text{Fe}_3\text{O}_4$ ,  $\text{NH}_2\text{-MIL-101(Cr)}$  and  $\text{Fe}_3\text{O}_4@\text{NH}_2\text{-MIL-101(Cr)}$  were confirmed on TEM and the images are presented in Fig. 4. The TEM image of  $\text{Fe}_3\text{O}_4$  (Fig. 4(a)) revealed well-dispersed spherical nanoparticles, which correspond with the TEM image of  $\text{Fe}_3\text{O}_4$  reported in recent studies by [44]. Figure 4(b) depicts a TEM image of octahedral

$\text{NH}_2\text{-MIL-101(Cr)}$ , which is morphologically similar to  $\text{MIL-101(Cr)}$  except for the surface roughness [34]. Figure 4(c) shows TEM image  $\text{Fe}_3\text{O}_4@\text{NH}_2\text{-MIL-101(Cr)}$  nanocomposite, revealing that  $\text{Fe}_3\text{O}_4$  nanoparticles are distributed on the surface of the octahedral topology, increasing the surface roughness. Furthermore, the agglomerated spherical  $\text{Fe}_3\text{O}_4$  nanoparticles were observed at the octahedral edges of the nanocomposite. The observed selected area electron diffraction (SAED) pattern in Fig. 4(d) corresponded with the diffraction patterns of  $\text{Fe}_3\text{O}_4$  [45], indicating that the  $\text{Fe}_3\text{O}_4$  nanoparticles were truly incorporated on the surface of  $\text{NH}_2\text{-MIL-101(Cr)}$ .

### 3.1.5 Point of Zero Charge

Point of zero charge (PZC) was evaluated using laboratory conducive pH drift method to get insight into the behaviour and surface chemistry of the prepared nanocomposite [46]. The obtained plot is depicted in Online Resource 6. According to Online Resource 6, the PZC of the nanocomposite was observed at pH 8.4, which postulates that the surface of the nanocomposite is positively charged below pH 8.4 and negatively charged above pH 8.4.

## 3.2 Optimisation Strategy

### 3.2.1 Screening of Factors Affecting MSPE of $\beta$ -Blockers Using Fractional Factorial Design

For every analytical sample preparation method, the screening process plays a significant role in evaluating the most controlling parameters for the extraction and preconcentration processes. This work screened five MSPME method

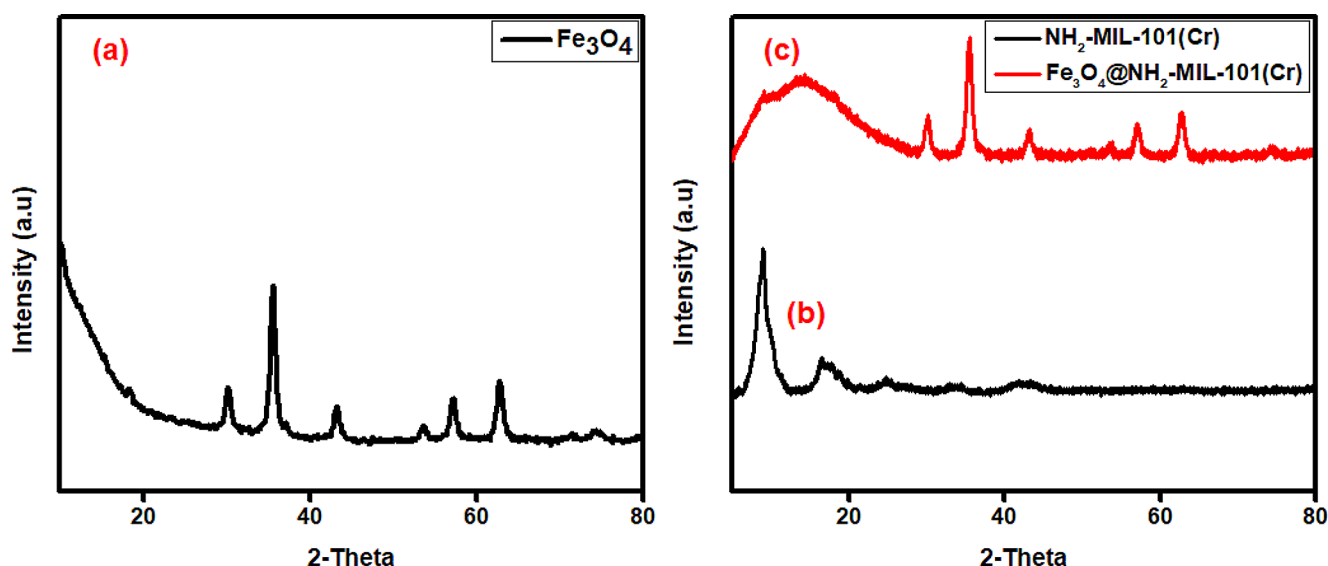
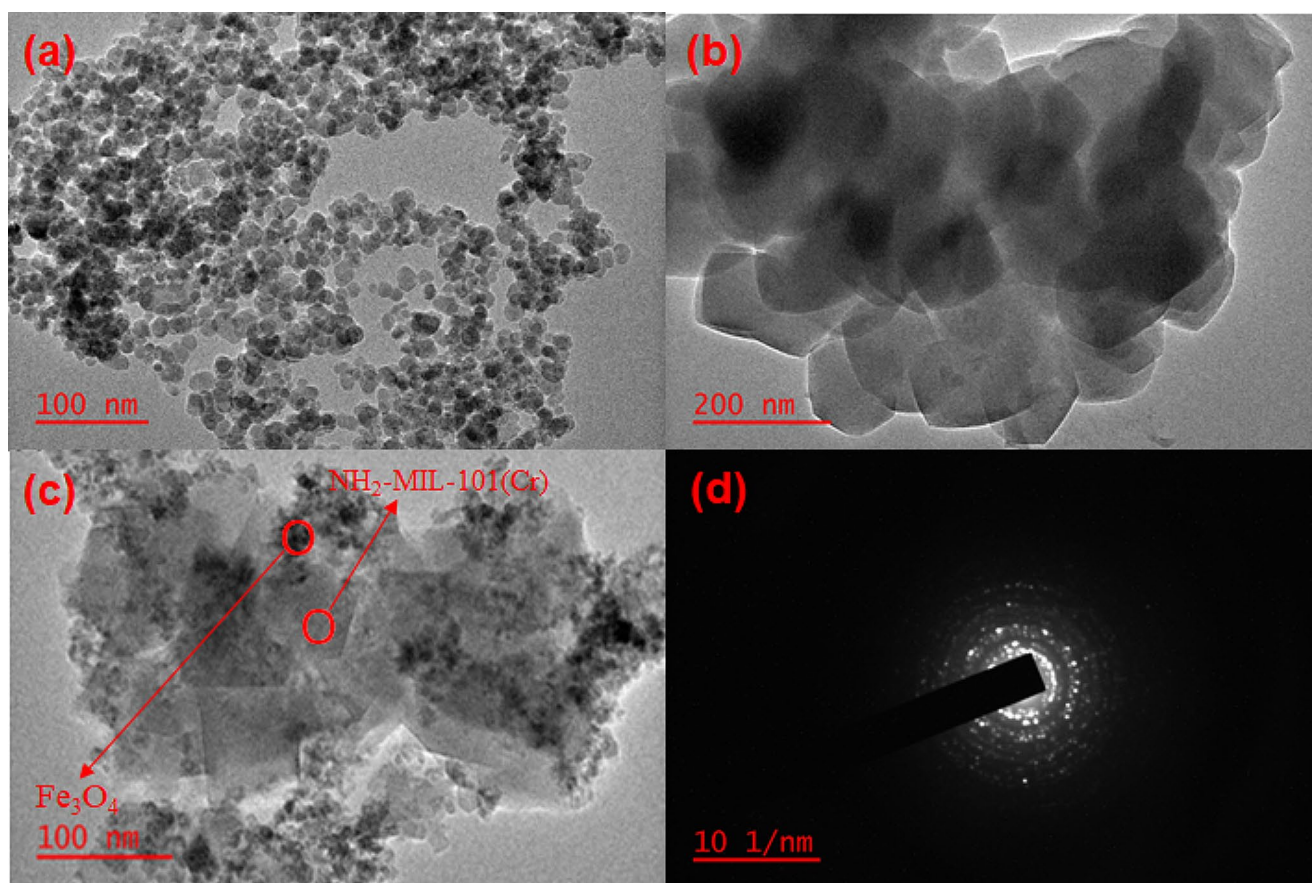


Fig. 3 XRD patterns of (a)  $\text{Fe}_3\text{O}_4$ , (b)  $\text{NH}_2\text{-MIL-101(Cr)}$  and (c)  $\text{Fe}_3\text{O}_4@\text{NH}_2\text{-MIL-101(Cr)}$



**Fig. 4** TEM images of (a)  $\text{Fe}_3\text{O}_4$ , (b)  $\text{NH}_2\text{-MIL-101(Cr)}$  and (c) TEM image and (d) SAED of  $\text{Fe}_3\text{O}_4@\text{NH}_2\text{-MIL-101(Cr)}$

parameters, such as MA, ET, DT, pH and EV, using two-level ( $2^{5-1}$ ) FFD. The screening procedure helps eliminate the parameters that are not influential towards any sample preparation method so that the number of experiments is reduced in the 2nd optimisation. Online Resource 1 shows the screened number of investigations and their respective percentage extraction recoveries (%ER). Analysis of variance (ANOVA) was used as a statistical formula to interpret the experimental data, and this data was presented as Pareto charts (Fig. 5). Pareto charts provide information about the main and interacting parameters' effect on the developed MSPE method. It consists of horizontal bars and a vertical red line, which indicates a 95% confidence level. If a bar corresponding to a particular factor obtained by liner models cuts through the red line, that factor is deemed significant towards the %ER at 95% confidence level [24].

Based on Fig. 5, only the bars corresponding to MA and pH crossed the red line indicating that these factors were statistically significant towards the extraction and preconcentration of ACE and MET. Further optimisation was conducted for these factors (pH and MA) using central composite design (CCD) based on response surface methodologies (RSM). This 2nd optimisation was performed to reduce

the number of experiments and further evaluate the interactive effects among these factors using quadratic equations [47].

### 3.2.2 Optimisation of the Most Influential Factor Using Central Composite Design

Further optimisation was conducted to investigate the interactive effects of the factors (EV and MA) that affected the MSPME method in the screening process. Optimisation parameters along their corresponding levels, including the extremes ( $\alpha$  values), are presented in Online Resource 2. The optimisation was carried out using CCD. The results involving 11 experiments and their corresponding %ER are shown in Online resource 3. The RSM based on CCD was used to evaluate the main, interactive and quadratic effects of the extraction and preconcentration of  $\beta$ -blockers [47]. The results are shown as 3D response surface plots in Fig. 6. Based on Fig. 6, significant interactions were observed between the optimised factors towards the extraction of both ACE and MET, i.e. when pH and MA increased, the maximum analytical response was observed. This is due to the abundance of active adsorption sites on the adsorbent



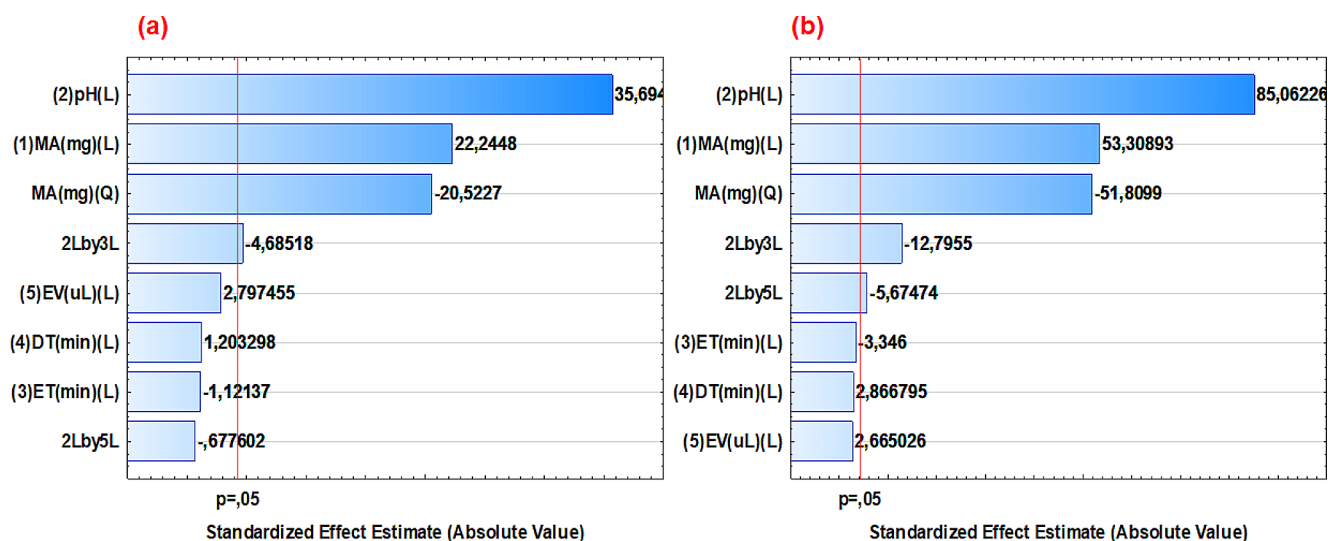


**Fig. 5** Pareto charts showing the significant factors in the extraction of (a) acebutolol and (b) metoprolol. 2Lby3L-interaction between pH and ET; 2Lby5L-interaction between pH and EV

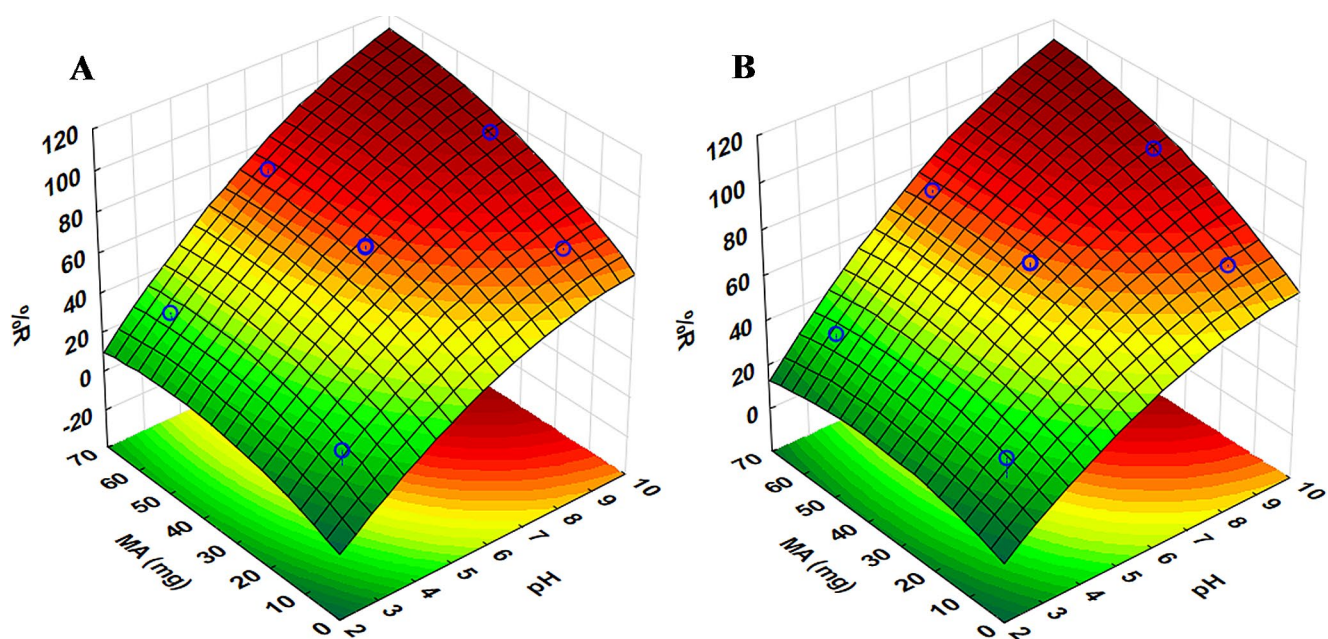


**Fig. 6** RSMs indicating the interactive effects between the optimised factors, (a) ACE and (b) MET. Optimized experimental conditions: Extraction time = 10 min; desorption time = 5 min and eluent volume = 500  $\mu$ L

when the amount is increased. For both ACE and MET, the highest preconcentration efficiency was attained when pH reached 9. The PZC of the nanocomposite was obtained at pH = 8.4, indicating that the surface of the nanocomposite is positive and negative below and above the PZC, respectively. Therefore, lower extraction efficiency obtained at lower pH values was due to the repulsion between the positively charged  $\text{Fe}_3\text{O}_4@ \text{NH}_2\text{-MIL-101}(\text{Cr})$  and the protonated ACE and MET. The acid dissociation constants ( $pK_a$ ) of ACE and MET are 9.67 and 9.7, respectively. At  $pH \leq pK_a$ , ACE and MET predominantly exist in protonated

forms and at  $pH \geq pK_a$ , the surfaces become neutral or negatively charged [48, 49]. According to the RSM and desirability functions, maximum extraction efficiency was obtained when pH exceeded PCZ and this could be explained based on the following phenomena: At  $pH \geq PZC$ , the surface of  $\text{Fe}_3\text{O}_4@ \text{NH}_2\text{-MIL-101}(\text{Cr})$  acquires negative charges and the surface of ACE and MET remain positively charged since the pH is still below their  $pK_a$  values. Therefore, electrostatic interactions occur between the nanocomposite and the selected  $\beta$ -blockers. When  $pH \leq pK_a$ , the surfaces of ACE and MET change and electrostatic repulsions drive the

nanocomposite and the selected  $\beta$ -blockers apart. However, desirability functions indicated that maximum extraction efficiency could still be obtained even when pH exceeded the pKa of ACE and MET. This suggests that electrostatic interactions were not only the mechanism controlling the extraction of the  $\beta$ -blockers.

However, RSM does not give precise experimental conditions but estimates the probable region. Therefore, further optimisation was conducted to acquire desirability profiles which present accurate optimum values for the optimised parameters.

Desirability profiles are plots that are obtained using statistical designs. Using these designs, the responses are statistically converted to dimensionless desirability values, which are then aggregated and used to get overall desirability. Theoretically, desirability profiles constitute three values which are 0, 0.5 and 1 for undesirable, partially desirable and desirable, respectively [50, 51]. The desirability profiles indicating the predicted values and desirability for both ACE and MET are presented in Fig. 7 and Online Resource

7. Additional theoretical information based on the desirability profiles can be obtained from our previously reported work [14]. Based on Fig. 7, it should be observed that both parameters had a significant effect on the extraction and pre-concentration of ACE and MET due to the reduced robustness of experimental data points. This indicates that minor changes on these points can considerably affect the %ER. A similar trend was observed on the desirability profile of MET (Online Resource 7). Optimum conditions obtained from RSM and desirability profiles were 64 mg and 9.4 for MA and pH, respectively. The screening process indicated that other parameters are not significant, including EV, ET and DT, which were kept at their best values of 500  $\mu$ L, 10 min and 5 min, respectively. The current analytical method exhibited observable merit and could potentially be used as a representative sample preparation method for extracting and preconcentrating a vast number of trace pollutants in the environment. Furthermore, the incorporated nano-adsorbent complemented the merit of the technique due to its high stability, great reusability and the ability to

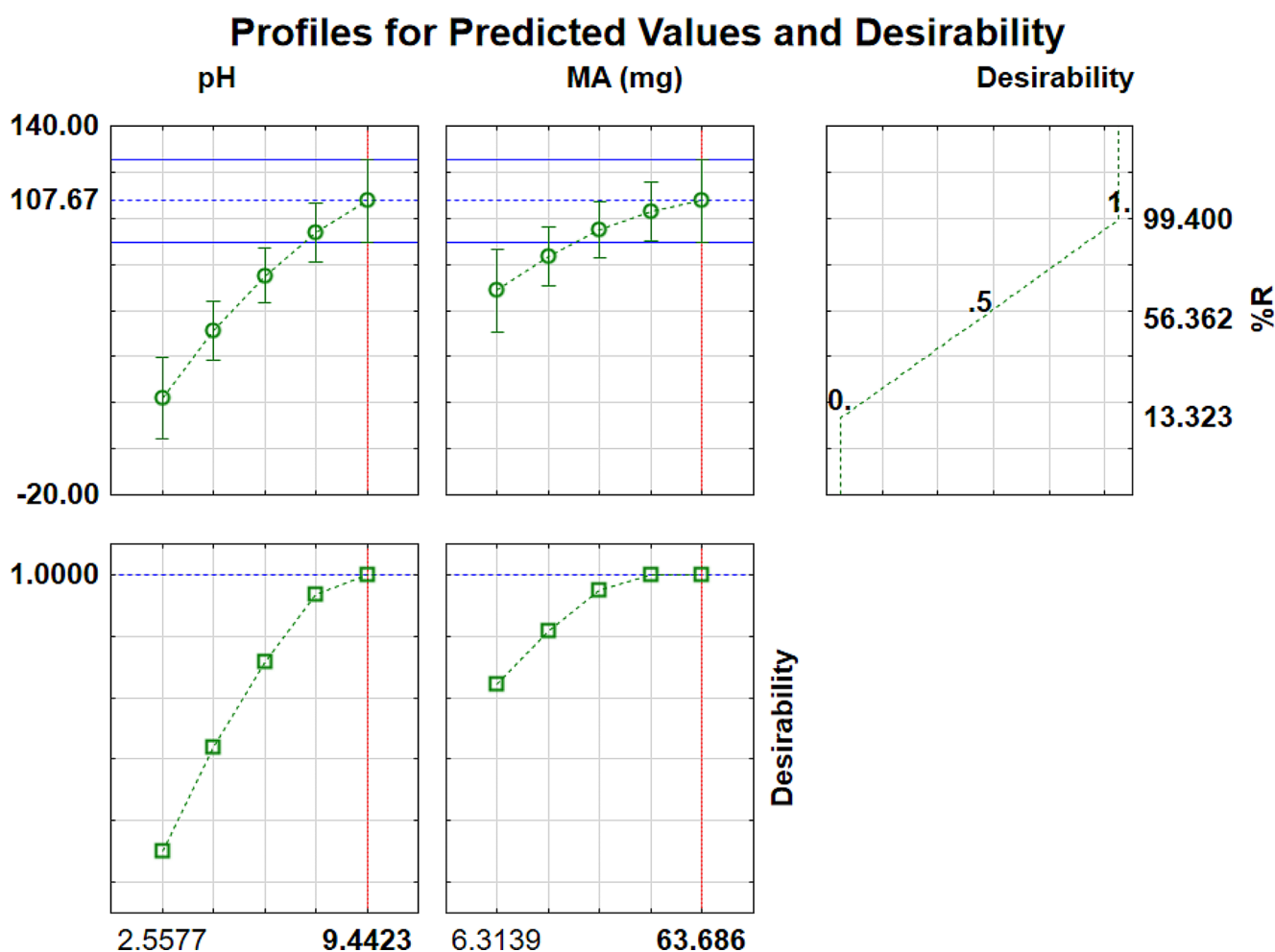


**Fig. 7** Desirability profile of ACE confirming the optimum conditions. Optimized experimental conditions: Extraction time = 10 min; desorption time = 5 min and eluent volume = 500  $\mu$ L; solution pH = 9.4 and mass of adsorbent = 64 mg

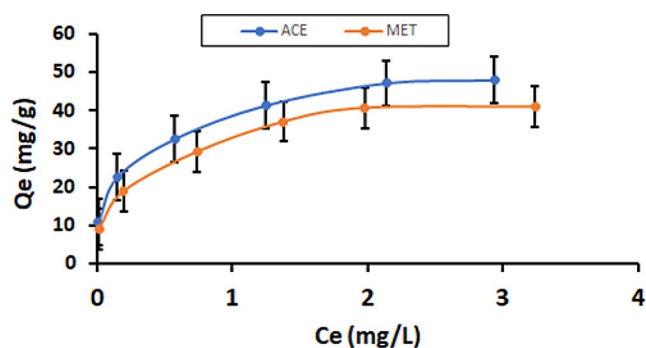


**Fig. 8** Adsorption isotherms of ACE and MET. Optimized experimental conditions: Extraction time = 10 min; desorption time = 5 min and eluent volume = 500  $\mu$ L; solution pH = 9.4 and mass of adsorbent = 64 mg

**Table 3** Adsorption isotherm models with the corresponding parameters

Models	Parameters	ACE	MET
Langmuir	$Q_m$ (mg g <sup>-1</sup> )	50.5	43.7
	$K_L$ (L mg <sup>-1</sup> )	5.21	4.67
	$R_L$	0.015–0.093	0.017–0.11
	$R^2$	0.9934	0.9927
Freundlich	$K_F$ (mg g <sup>-1</sup> )	44.5	32.2
	$n$	3.0	1.9
	$R^2$	0.9185	0.9152
Dubinin-Radushkevich (D-R)	$Q_{D-R}$ (mg g <sup>-1</sup> )	46.6	39.4
	$\beta$ (mol <sup>2</sup> J <sup>-2</sup> )	$3.00 \times 10^{-7}$	$4 \times 10^{-7}$
	$E$ (kJ mol <sup>-1</sup> )	4.08	3.54
	$R^2$	0.9785	0.951
Sips	$K_s$ (L mg <sup>-1</sup> )	0.073	0.041
	$Q_{max}$ (mg g <sup>-1</sup> )	47.9	41.1
	$n_s$	1.01	0.97

efficiently adsorb and desorb the selected  $\beta$ -blockers in a short space of time.

### 3.3 Adsorption Isotherms and Capacity

Adsorption isotherms are necessary to understand the adsorbent and analyte interaction mechanism (Fig. 8). In the adsorption mechanism, the equilibrium phenomena are evaluated to obtain the adsorption capacity of the adsorbent concerning the amount of the analytes adsorbed onto the adsorbent relative to the amount left in the solution at equilibrium. The experimental adsorption capacities were 47.9 and 41.1 mg g<sup>-1</sup> for ACE and MET, respectively. The adsorption isotherm data were fitted to four models to understand further the adsorption mechanism (Langmuir, Freundlich, Dubinin-Radushkevich and Sips models) [36]. The model parameters and equations are presented in Table 3 and Online Resource 4, respectively. The model that best fits the adsorption isotherm data was selected based on the correlations of determination ( $R^2$  values).

The results indicate that the Langmuir model (Table 3, Online Resource 8) better describes the adsorption mechanism than Freundlich (Table 3, Online Resource 9) based on higher  $R^2$  values obtained for both ACE and MET. The validity of the Langmuir model was further supported by the calculated adsorption capacities of 47.9 and 41.1 mg g<sup>-1</sup>, comparable to the experimental adsorption capacities of 50.51 and 43.67 mg g<sup>-1</sup> for ACE and MET, respectively. This indicated that the adsorption of ACE and MET formed a single layer onto the homogeneously distributed active sites on the surface of Fe<sub>3</sub>O<sub>4</sub>@NH<sub>2</sub>-MIL-101(Cr) [52]. To understand whether the interaction between the  $\beta$ -blockers and Fe<sub>3</sub>O<sub>4</sub>@NH<sub>2</sub>-MIL-101(Cr) is based on physical or chemical interactions, the experimental isotherm data were fitted to the Dubin-Radushkevich model (Table 3, Online Resource 10). Based on the results obtained, the mean free energies ( $E$  (kJ mol<sup>-1</sup>)) were below 8 kJ mol<sup>-1</sup> embracing physisorption as the dominating type of interaction. The validity of the Langmuir was further confirmed by the Sips isotherm model (Table 3, Online Resource 11). This model is derived from the combination of Langmuir and Freundlich models. The heterogeneity constant ( $n$ ) is the model's most imperative parameter, indicating that if  $n$  is between 0 and 1, Sips equation reduces to Freundlich, and if  $n$  is closer or equal to 1, Sips equation reduces to Langmuir [52]. Based on the results obtained in Table 3,  $n$  values were close to unity for both ACE and MET, supporting the validity of the Langmuir model.

### 3.4 Regenerability and Reusability

Experiments were performed to test the adsorbent's stability, regenerability and reusability. The reusability of an adsorbent prevails as an attractive feature, making the adsorption technology cheaper and feasible. This study performed the regenerability and reusability studies to evaluate how often the already used Fe<sub>3</sub>O<sub>4</sub>@NH<sub>2</sub>-MIL-101(Cr) nanocomposite can be utilised whilst preserving maximum analytical response (%ER). The results shown in Fig. 9 indicates that the nanocomposite can be repeatedly used about eight times, maintaining  $\geq 89\%$  extraction recoveries for both ACE and MET. Furthermore, the %RSDs for the reusability studies were below 3.2%, indicating good precision. Regardless of a slight collapse in adsorption efficiency, the spent nano-adsorbent exhibited superior stability, regenerability and reusability. Based on the reusability performance of Fe<sub>3</sub>O<sub>4</sub>@NH<sub>2</sub>-MIL-101(Cr) nanocomposite, it can be concluded that the nanocomposite could be potentially incorporated in various sample preparation techniques for the enrichment of various environmental pollutants.

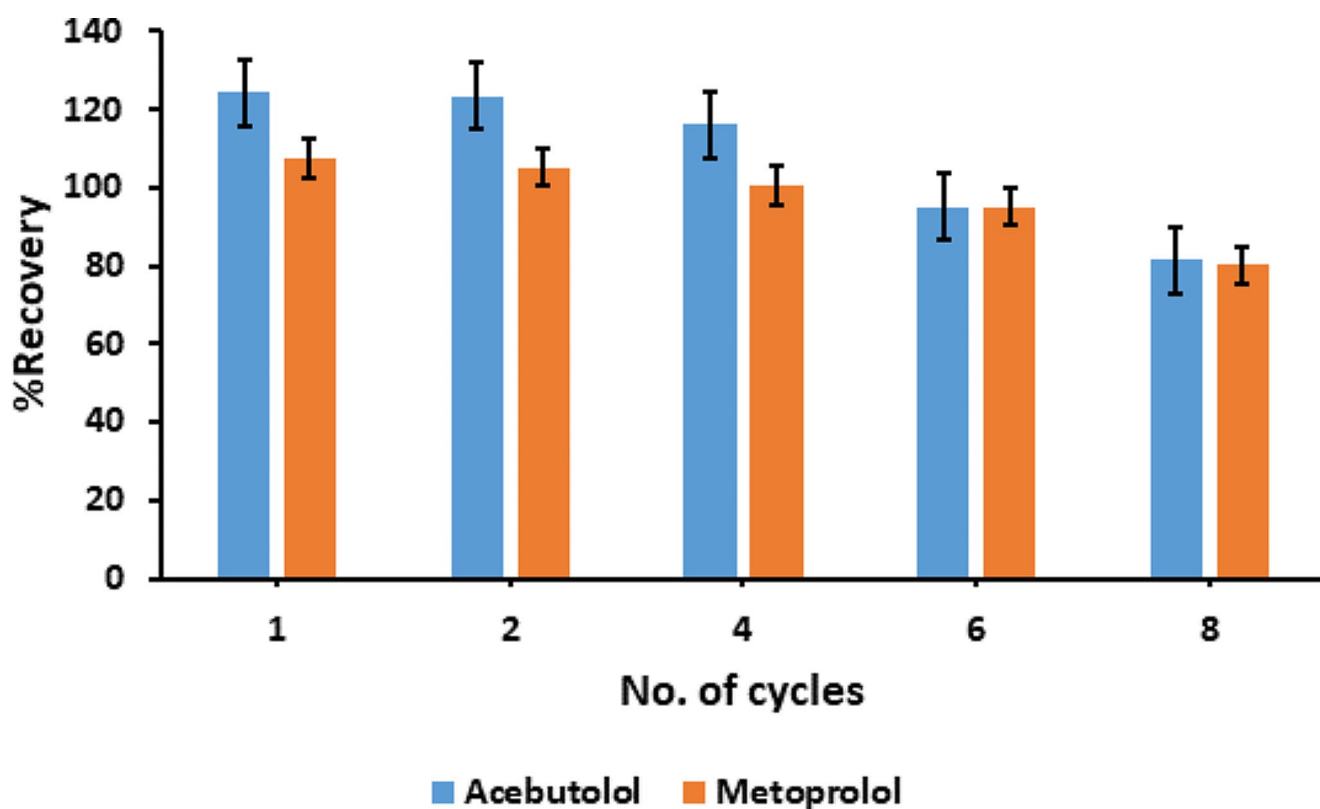


**Fig. 9** Reusability studies of Fe<sub>3</sub>O<sub>4</sub>@NH<sub>2</sub>-MIL-101(Cr): Optimum conditions: MA=64; pH=9.4; ET=10 min, DT=10 min and EV=500  $\mu$ L. Optimized experimental conditions: Extraction

time = 10 min; desorption time = 5 min and eluent volume = 500  $\mu$ L; solution pH = 9.4 and mass of adsorbent = 64 mg

### 3.5 Method Validation

Under best experimental conditions, the analytical figures of merit for the developed MSPME method were evaluated using limit of detection (LOD), limit of quantification (LOQ), preconcentration factor (PF), repeatability (intra-day), reproducibility (inter-day) and linearity (Table 4). Firstly, the calibration curves for each analyte were plotted, and the MSPME method was used to preconcentrate the standard solutions of  $\beta$ -blockers with concentrations ranging from 200 to 1200  $\mu$ g L<sup>-1</sup>. The linearity and correlations of determination obtained from the calibration curves are also shown in Table 4. The linearity range was good, indicating outstanding method performance. LODs and LOQs are the smallest amounts that can increase the original signal sensitivity by a factor of 3 and 10, respectively [15]. They are obtained by dividing the standard deviation by the gradient of the calibration curve. The obtained LODs and LOQs for ACE and MET are also shown in Table 4. The preconcentration factor (PF), expressed as the ratio of the sample volume to the eluent volume, was 10. The intra-day and inter-day studies were performed to evaluate the precision of the MSPME method. These studies were conducted based on ten repetitions on the same (repeatability,  $n = 10$ )

and six different days (reproducibility,  $n = 6$ ). The obtained results were demonstrated regarding relative standard deviations (RSDs). The intra-day and inter-day precisions were less than 1% and 2%, respectively. This indicated that the method could potentially be applied for the preconcentration of many environmental pollutants and is reproducible. The specificity and selectivity of the MSPME method was demonstrated by comparing the stability and similarity of the analyte peaks in both spiked river water sample and spiked ultrapure water from the lab (Fig. 10).

According to the results obtained in Fig. 10, the retention times and the peaks were similar with SD of 0.0076, confirming the specificity of the method for ACE and MET. The matrix effect on the developed method was evaluated based on the trend reported previously, i.e. when  $\%ME \leq 20\%$  or  $\%ME \geq -20\%$ , the matrix shows no effect, when  $20\% \geq \%ME \leq 50\%$  or  $-50\% \leq \%ME \leq -20\%$ , the matrix has moderate effect and when  $\%ME \leq -50\%$  or  $\%ME \geq 50\%$ , the matrix effect is extremely significant [53, 54]. The results obtained indicated that the  $\%ME$  was below 20% (Table 4) for both analytes ACE and MET, which suggested that the matrix effect was negligible towards the performance of the method. Based on the literature, the response of the detector is improved when the  $\%ME$  is positive and visa

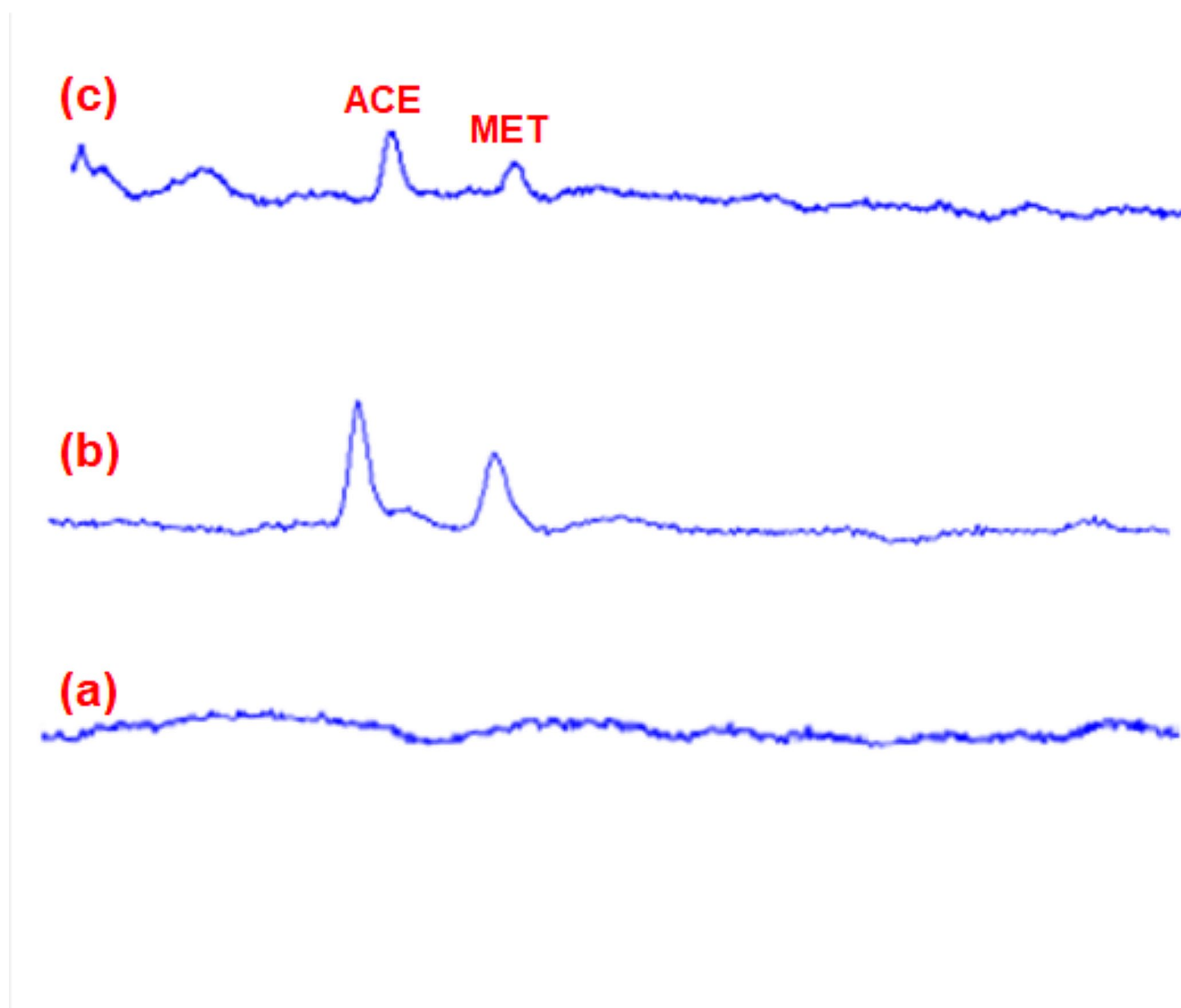


**Fig. 10** Chromatograms of (a) blank sample, (b) spiked ultrapure water and (c) spiked river water

**Table 4** Method validation for the extraction and preconcentration of ACE and MET

Parameter	ACE	MET
Linearity	0.2–1200	0.2–1200
R <sup>2</sup>	0.9987	0.9968
LOD ( $\mu\text{g L}^{-1}$ )	0.057	0.065
LOQ ( $\mu\text{g L}^{-1}$ )	0.19	0.22
Repeatability (%RSD)	0.63	0.74
Reproducibility (%RSD)	1.06	1.18
PF	10	10
%Matrix effect (%ME)	2.47	2.92

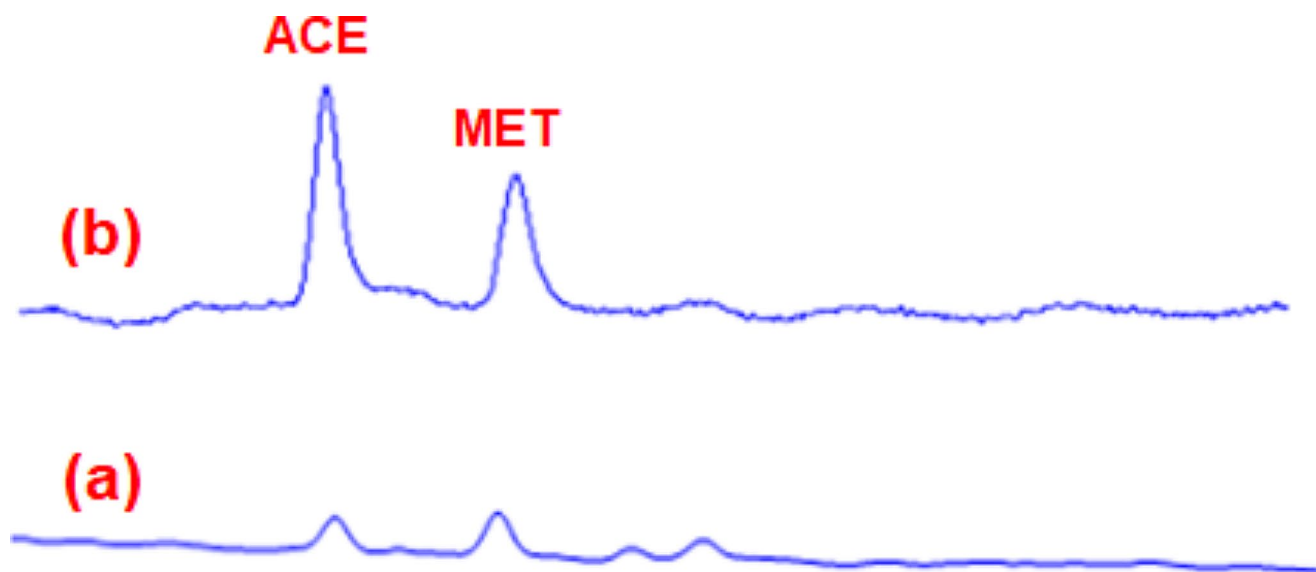
versa [55]. The obtained %ME was also positive further confirming that the matrix had no effect on the merit of the developed method.

### 3.6 Application to Real Samples

The feasibility of the MSPE method was investigated using spiked water matrices (river, influent and effluent water samples). The spiking was conducted at two levels, a lower level ( $200 \mu\text{g L}^{-1}$ ) and a higher level  $800 \mu\text{g L}^{-1}$  for both ACE and MET (Table 5). The samples were analysed in triplicates, and the overall results were averaged. The results indicated that the MSPE method could perform effectively even in the presence of interfering species, with %ER ranging from 93.2 to 99.1%. This suggested that matrix interferences had no obvious drawback on the extraction and preconcentration of the selected  $\beta$ -blockers. This was supported by the %RSD, which was less than 10%, further proving that the effects from the matrices were insignificant for the developed analytical method. The MSPE method

**Table 5** Application of MSPE method in real samples (mean  $\pm$  SD)

Samples	Spiked levels (Added, $\mu\text{g L}^{-1}$ )	Acebutolol			Metoprolol		
		Found ( $\mu\text{g L}^{-1}$ )	%RSD	%R	Found ( $\mu\text{g L}^{-1}$ )	%RSD	%R
Influent	0	$1.11 \pm 0.06$	5.4	-	$13.8 \pm 0.66$	4.8	-
	200	$188 \pm 9$	4.8	93.2	$203 \pm 8$	3.9	94.8
	800	$766 \pm 25$	3.3	95.6	$787 \pm 21$	2.7	96.7
Effluent	0	$0.121 \pm 0.007$	5.8	-	$0.338 \pm 0.015$	4.4	-
	200	$190 \pm 8$	4.2	94.9	$192 \pm 9$	4.7	95.7
	800	$772 \pm 23$	3.0	96.5	$783 \pm 19$	2.4	97.8
River water	0	ND	-	-	ND	-	-
	200	$197 \pm 9$	4.6	98.7	$195 \pm 7$	3.6	97.5
	800	$793 \pm 26$	3.3	99.1	$790 \pm 27$	3.4	98.7

**Fig. 11** Chromatograms of the (a) spiked river water sample and (b) after pre-concentration

exhibited great potential for the matrix clean-up, extraction and pre-concentration of  $\beta$ -blockers from different environmental waters. Figure 11 illustrates the chromatograms of the ACE and MET for the spiked river water sample and after the pre-concentration. The pre-concentrated peaks are enhanced, indicating successful pre-concentration and matrix cleanup. Herein, the river water sample was used as a representative to demonstrate the performance of the method in all real water samples.

### 3.7 Comparison of the Proposed Method with Other Methods in the Literature

To evaluate the performance, feasibility, and reliability of the proposed MSPME analytical method, comparison studies were conducted with other methods reported in the literature for the pre-concentration of  $\beta$ -blockers in various environmental matrices. The comparison was based on the linearity, LODs and %RSD. The results are shown in Table 6. The results indicated that the proposed method had reasonably

wider linearity, good repeatability and reproducibility. The LODs for the method in question were comparably lower than those of other reported methods. This indicated that the proposed MSPME method is sensitive, rapid, facile, environmentally friendly, and ideal for the enrichment of  $\beta$ -blockers from different environmental matrices. The merit of the method was further observed when a higher %ER for both  $\beta$ -blockers were obtained regardless of the presence of interfering substances. Moreover, the optimum %ER were still obtained after eight consecutive cycles.

## 4 Conclusion

In conclusion,  $\text{NH}_2$ -MIL-101(Cr) doped magnetic nanoparticles were fabricated and used in the MSPME method to enrich and determine the selected  $\beta$ -blockers (ACE and MET) in the model and real water samples. The  $\text{Fe}_3\text{O}_4@$  $\text{NH}_2$ -MIL-101(Cr) nanocomposite was characterised and confirmed by the following analytical techniques:

**Table 6** Performance comparative studies of the proposed method with previously reported methods

Analytes	Matrix	Analytical method	Linearity ( $\mu\text{g L}^{-1}$ )	LODs ( $\mu\text{g L}^{-1}$ )	%RSD	References
Acebutolol, metoprolol, atenolol, propranolol	Influent and effluent samples	SPE/LC/MS-MS	1-500	0.006–0.011	5–7	[56]
Metoprolol, pindolol, acebutolol, labetalol, atenolol	Human urine	SPE/HPLC-DAD	10–100 0	0.6-2.0	2–4	[57]
Metoprolol, propranolol	Human plasma	Tandem DLLME/HPLC-UV	2.5–2500	0.12–0.33	~5.7	[58]
Acebutolol, propranolol, labetalol	Distilled and wastewater effluents	SPE and LC-MS/MS	50-2000	1.3-5.0	6.2–13.0	[59]
Acebutolol, metoprolol, atenolol	Human urine	SPE and HPLC-MS/MS	-	10–17	-	[60]
Acebutolol, propranolol, labetalol	Wastewater effluents and natural waters	Dispersive SPE and LC-DAD	-	0.006–0.02	3.3–7.6	[61]
Metoprolol, pindolol, propranolol, betaxolol	Serum	LIS-PP-SHLE/UHPLC-MS-MS	5-100	0.4–1.5	< 11	[62]
Acebutolol, metoprolol	Influent, effluent and river water samples	MSPE	0.3–1200	0.06–0.07	0.63–1.18	This method

SPE: Solid-phase extraction; LC: Liquid chromatography; MS: Mass spectrometry; MS/MS: Tandem mass spectrometry; HPLC: High pressure liquid chromatography; DAD: Diode array detector; DLLMP: Dispersive liquid-liquid micro-extraction, UV: Ultraviolet; LIS: Lab-In-Syringe; PP: Protein precipitation; SHLE: Salting-out homogeneous liquid-liquid extraction; UHPLC: Ultra-high performance liquid chromatography

XRD, FTIR, SEM, BET, TEM and VSM. The developed MSPE method showed eminent potential as a sample preparation method for the chosen  $\beta$ -blockers. Before applying the MSPE method in real samples, parameters deemed affecting the extraction were first screened using FFD in model solutions. Furthermore, the most significant parameters obtained in the screening process were further optimised using CCD. At optimum conditions, the LODs and LOQs used to assess the performance and reliability of the MSPE method were  $\leq 0.065$  and  $\leq 1.178 \mu\text{g L}^{-1}$  for ACE and MET, respectively. The regenerability and reusability studies indicated that the MSPME method could still be reliably applied at least eight times, indicating high stability and reusability of the nanocomposite. The MSPE method was then used to extract and preconcentrate  $\beta$ -blockers in real water samples. Higher %ER values were still obtained in these real samples indicating that the matrix interferences had no significant effect on the method's performance. The above-mentioned fascinating features indicate that  $\text{Fe}_3\text{O}_4@ \text{NH}_2\text{-MIL-101}$  (Cr) nanoadsorbent could potentially solve global challenges based on monitoring the pollutants in the environmental wastewater and the ultimate remediation.

**Supplementary Information** The online version contains supplementary material available at <https://doi.org/10.1007/s42250-024-00969-4>.

**Acknowledgements** The authors are grateful to the University of Johannesburg for granting us the space in their laboratories to make this work possible. The gratitude is further extended to other research facilities such as Council for Scientific and Industrial Research (CSIR) for allowing us to use some of their analytical techniques.

**Authors' contributions** NJW contributed in conceptualization, method development, synthesis, characterization, conducting experiments, experimental design, data interpretation, writing original manuscript and

editing. AM and SKS contributed in data interpretation, experimental design, proofreading and editing. PNN contributed in conceptualization, project administration software, investigation, experimental design, editing and supervision. YZ contributed in editing, reviewing the manuscript and supervision. All authors read and approved the final manuscript.

**Funding** The authors are grateful to Department of Science and Innovation- National Research Foundation South African Research Chairs Initiative (DSI-NRF SARChI) funding instrument (grant no. 91230) for financial support.

Open access funding provided by University of Johannesburg.

## Declarations

**Ethical Approval** Not applicable.

**Informed Consent** Not applicable.

**Open Access** This article is licensed under a Creative Commons Attribution 4.0 International License, which permits use, sharing, adaptation, distribution and reproduction in any medium or format, as long as you give appropriate credit to the original author(s) and the source, provide a link to the Creative Commons licence, and indicate if changes were made. The images or other third party material in this article are included in the article's Creative Commons licence, unless indicated otherwise in a credit line to the material. If material is not included in the article's Creative Commons licence and your intended use is not permitted by statutory regulation or exceeds the permitted use, you will need to obtain permission directly from the copyright holder. To view a copy of this licence, visit <http://creativecommons.org/licenses/by/4.0/>.

## References

- aus der T, Beek et al (2016) Pharmaceuticals in the environment—global occurrences and perspectives. *Environ Toxicol Chem* 35(4):823–835

2. Rodríguez-Llorente D et al (2023) Extraction of pharmaceuticals from hospital wastewater with eutectic solvents and terpenoids: computational, experimental, and simulation studies. *Chem Eng J* 451:138544
3. Xu J, Wang Y, Sun H, Zhang W (2022) Adsorption and leaching of  $\beta$ -blockers in fluvo-aquic and black soil: Behavior characteristic and enantiomer selectivity. *Environ Res* 214:114062
4. Uzelac MM, Armaković SJ, Armaković S, Četojević-Simin DD, Agbaba J, Banić ND (2022) The role of environmental waters ionic composition and UV-LED radiation on photodegradation, mineralization and toxicity of commonly used  $\beta$ -blockers. *J Mol Struct* 1249:131579
5. Yi M, Sheng Q, Sui Q, Lu H (2020)  $\beta$ -blockers in the environment: distribution, transformation, and ecotoxicity. *Environ Pollut* 266:115269
6. Xie P et al (2019) Application of vacuum-ultraviolet (VUV) to degrade  $\beta$ -blocker propranolol in aquatic environment: efficiency, kinetics, pathways and acute toxicity. *J Taiwan Inst Chem Eng* 103:75–84
7. Farzam K, Jan A (2022) Beta blockers. in StatPearls [Internet]. StatPearls Publishing
8. Jones OAH, Voulvoulis N, Lester JN (2005) Human pharmaceuticals in wastewater treatment processes. *Crit Rev Environ Sci Technol* 35(4):401–427
9. et al., The Visible-Light-Driven Activity of Biochar-Doped TiO<sub>2</sub> Photocatalysts in  $\beta$ -Blockers Removal from Water, *Materials*, vol. 16, no. 3. 2023. doi: 10.3390/ma16031094
10. Mashile PP, Nomngongo PN (2021) Magnetic cellulose-chitosan nanocomposite for simultaneous removal of emerging contaminants: Adsorption Kinetics and Equilibrium studies. *Gels* 7(4). <https://doi.org/10.3390/gels7040190>
11. Kumar R et al (2022) A review on emerging water contaminants and the application of sustainable removal technologies. *Case Stud Chem Environ Eng* 6:100219. <https://doi.org/10.1016/j.csee.2022.100219>
12. Yıldırım S, Erkmén C, Uslu B (2022) Novel trends in analytical methods for  $\beta$ -blockers: an overview of applications in the last decade. *Crit Rev Anal Chem* 52(1):131–169
13. Abadi MAA, Masroumia M, Abedi MR (2021) Simultaneous extraction and preconcentration of three Beta ( $\beta$ )-blockers in biological samples with an efficient magnetic dispersive micro-solid phase extraction procedure employing in situ sorbent modification. *Microchem J* 163:105937
14. Waleng NJ, Selahle SK, Mpupa A, Nomngongo PN (2022) Development of dispersive solid-phase microextraction coupled with high-pressure liquid chromatography for the preconcentration and determination of the selected neonicotinoid insecticides. *J Anal Sci Technol* 13(1):1–15
15. Lefatle MC et al (2022) Preparation, characterization, and application of chitosan-kaolin-based nanocomposite in magnetic solid-phase extraction of tetracycline in aqueous samples. *Chem Pap*, pp. 1–18
16. Selahle SK, Waleng NJ, Mpupa A, Nomngongo PN (2020) Magnetic solid phase extraction based on nanostructured magnetic porous porphyrin organic polymer for simultaneous extraction and preconcentration of neonicotinoid insecticides from surface water. *Front Chem* 8:555847
17. Masini JC, do Nascimento FH, Vitek R (2021) Porous monolithic materials for extraction and preconcentration of pollutants from environmental waters. *Trends Environ Anal Chem* 29:e00112
18. Durak BY, Chormey DS, Firat M, Bakirdere S (2020) Validation of ultrasonic-assisted switchable solvent liquid phase microextraction for trace determination of hormones and organochlorine pesticides by GC-MS and combination with QuEChERS. *Food Chem* 305:125487
19. Wang H et al (2022) Analysis of  $\beta$ -blockers and  $\beta$ 2-agonists in environmental and biological samples by magnetic solid-phase extraction combined with high-performance liquid chromatography-tandem mass spectrometry. *J Sep Sci* 45(13):2321–2333
20. Jouyban A, Farajzadeh MA, Mogaddam MRA (2020) In matrix formation of deep eutectic solvent used in liquid phase extraction coupled with solidification of organic droplets dispersive liquid-liquid microextraction; application in determination of some pesticides in milk samples. *Talanta* 206:120169
21. Bodur S, Erarpat S, Bakirdere S (2020) Fe<sub>3</sub>O<sub>4</sub>/reduced graphene oxide nanocomposites based dispersive solid phase microextraction for trace determination of profenofos in white rice flour samples. *J Food Compos Anal* 91:103516
22. Soylak M, Ozalp O, Uzcan F (2021) Magnetic nanomaterials for the removal, separation and preconcentration of organic and inorganic pollutants at trace levels and their practical applications: a review. *Trends Environ Anal Chem* 29:e00109
23. Selahle SK, Mpupa A, Nqombolo A, Nomngongo PN (2022) A nanostructured o-hydroxyazobenzene porous organic polymer as an effective sorbent for the extraction and preconcentration of selected hormones and insecticides in river water. *Microchem J* 181:107791
24. Alhmaunde A, Masroumia M, Javid A (2022) Facile synthesis of new magnetic sorbent based on MOF-on-MOF for simultaneous extraction and determination of three benzodiazepines in various environmental water samples using dispersive micro solid-phase extraction and HPLC. *Microchem J* 181:107802
25. Bozyiğit GD et al (2022) Polystyrene-coated Magnetite nanoparticles based Dispersive Micro-solid phase extraction of active Pharmaceutical ingredients of antidepressant drugs and determination by GC-MS. *ChemistrySelect* 7(10):e202104435
26. Chen L et al (2022) Covalent organic framework-based magnetic solid phase extraction coupled with micellar electrokinetic chromatography for the analysis of trace organophosphorus pesticides in environmental water and atmospheric particulates. *J Chromatogr A* 1673:463030
27. Sereshti H, Karami F, Nouri N, Farahani A (2021) Electrochemically controlled solid phase microextraction based on a conductive polyaniline-graphene oxide nanocomposite for extraction of tetracyclines in milk and water. *J Sci Food Agric* 101(6):2304–2311
28. Ben Attig J, Latrous L, Zougagh M, Ríos Á (2021) Ionic liquid and magnetic multiwalled carbon nanotubes for extraction of N-methylcarbamate pesticides from water samples prior their determination by capillary electrophoresis. *Talanta* 226:122106
29. Bahrani S, Ghaedi M, Dashtian K, Ostovan A, Mansoorkhani MJK, Salehi A (2017) MOF-5 (Zn)-Fe<sub>2</sub>O<sub>4</sub> nanocomposite based magnetic solid-phase microextraction followed by HPLC-UV for efficient enrichment of colchicine in root of colchicum extracts and plasma samples. *J Chromatogr B* 1067:45–52
30. Manshadi SS, Dadfarnia S, Shabani AMH, Afsharipour R, Jabbaran S (2022) S and N co-doped graphene quantum dots as an effective fluorescence probe for sensing of furazolidone after magnetic solid-phase microextraction using magnetic multiwalled carbon nanotubes. *Microchem J* 179:107439
31. Hashemi B, Zohrabi P, Raza N, Kim K-H (2017) Metal-organic frameworks as advanced sorbents for the extraction and determination of pollutants from environmental, biological, and food media. *TrAC Trends Anal Chem* 97:65–82
32. Kumar P, Bansal V, Kim K-H, Kwon EE (2018) Metal-organic frameworks (MOFs) as futuristic options for wastewater treatment. *J Ind Eng Chem* 62:130–145
33. Silva M, Morante-Zarcero S, Pérez-Quintanilla D, Sierra I (2019) Simultaneous determination of pindolol, acebutolol and metoprolol in waters by differential-pulse voltammetry using an efficient sensor based on carbon paste electrode modified with



- amino-functionalized mesostructured silica. *Sens Actuators B Chem* 283:434–442. <https://doi.org/10.1016/j.snb.2018.12.058>
34. Cai Y et al (2021) Efficient capture of  $\text{ReO}_4^-$  on magnetic amine-functionalized MIL-101(cr): revealing from selectivity to mechanism. *Sci Total Environ* 771:144840. <https://doi.org/10.1016/j.scitotenv.2020.144840>
  35. Mehrabadi Z, Faghihian H (2018) Comparative photocatalytic performance of  $\text{TiO}_2$  supported on clinoptilolite and  $\text{TiO}_2/\text{Salicylaldehyde-NH}_2\text{-MIL-101 (cr)}$  for degradation of pharmaceutical pollutant atenolol under UV and visible irradiations. *J Photochem Photobiol Chem* 356:102–111
  36. Ayawei N, Ebelegi AN, Wankasi D (2017) Modelling and interpretation of adsorption isotherms, *J. Chem.*, vol. 2017
  37. Martinez-Tamayo E, Beltran-Porter A, Beltran-Porter D (1986) Iron compounds in high oxidation states: II. Reaction between  $\text{Na}_2\text{O}_2$  and  $\text{FeSO}_4$ . *Thermochim Acta* 97:243–255
  38. Shafiei M, Alivand MS, Rashidi A, Samimi A, Mohebbi-Kalhari D (2018) Synthesis and adsorption performance of a modified micro-mesoporous MIL-101 (cr) for VOCs removal at ambient conditions. *Chem Eng J* 341:164–174
  39. Sun X, Xia Q, Zhao Z, Li Y, Li Z (2014) Synthesis and adsorption performance of MIL-101 (cr)/graphite oxide composites with high capacities of n-hexane. *Chem Eng J* 239:226–232
  40. Hartmann M, Fischer M (2012) Amino-functionalized basic catalysts with MIL-101 structure. *Microporous Mesoporous Mater* 164:38–43
  41. Li X-Y, Ding W-Q, Liu P, Xu L, Fu M-L, Yuan B (2023) Magnetic  $\text{Fe}_3\text{O}_4/\text{MIL-101}$  composite as a robust adsorbent for removal of p-arsanilic acid and roxarsenic in the aqueous solution. *Colloids Surf Physicochem Eng Asp* 662:131014
  42. Walia S, Kaur M, Kansal SK (2022) Adsorptive removal of 2,4-dinitrophenol from aqueous phase using amine functionalized metal organic framework ( $\text{NH}_2\text{-MIL-101(cr)}$ ). *Mater Chem Phys* 289:126493. <https://doi.org/10.1016/j.matchemphys.2022.126493>
  43. Shi H, Li C, Wang L, Wang W, Bian J, Meng X (2023) Efficient photocatalytic degradation of ammonia nitrogen by Z-scheme  $\text{NH}_2\text{-MIL-101(Fe)/BiVO}_4$  heterostructures. *J Alloys Compd* 933:167815. <https://doi.org/10.1016/j.jallcom.2022.167815>
  44. Selahle SK, Mpupa A, Nomngongo PN (2022) Liquid chromatographic determination of per- and polyfluoroalkyl substances in environmental river water samples. *Arab J Chem*, p. 103960
  45. Zhang N, Huang Y, Wang M (2018) 3D ferromagnetic graphene nanocomposites with  $\text{ZnO}$  nanorods and  $\text{Fe}_3\text{O}_4$  nanoparticles co-decorated for efficient electromagnetic wave absorption. *Compos Part B Eng* 136:135–142
  46. Tang Y, Chen Z, Wen Q, Liu B, Huang X (2022) Magnetic powdery acrylic polymer with ultrahigh adsorption capacity for atenolol removal: Preparation, characterization, and microscopic adsorption mechanism. *Chem Eng J* 446:137175. <https://doi.org/10.1016/j.cej.2022.137175>
  47. Ghorbani M et al (2019) Ultrasonic assisted magnetic dispersive solid phase microextraction for preconcentration of two non-steroidal anti-inflammatory drugs in real water, biological and milk samples employing an experimental design. *Microchem J* 145:1026–1035. <https://doi.org/10.1016/j.microc.2018.12.019>
  48. Raoufi A, Ebrahimi M, Bozorgmehr MR (2019) Application of response surface modeling and chemometrics methods for the determination of Atenolol, Metoprolol and Propranolol in blood sample using dispersive liquid–liquid microextraction combined with HPLC-DAD. *J Chromatogr B* 1132:121823
  49. Shi W, Chu Y, Xia M, Wang F, Fu C (2021) The adsorption performance and micro-mechanism of  $\text{MoS}_2/\text{montmorillonite}$  composite to atenolol and acebutolol: adsorption experiments and a novel visual study of interaction. *Ecotoxicol Environ Saf* 213:111993
  50. Bezerra MA et al (2019) Simultaneous optimization of multiple responses and its application in analytical chemistry—a review. *Talanta* 194:941–959
  51. Valasques GS et al (2020) Multivariate optimization for the determination of cadmium and lead in crude palm oil by graphite furnace atomic absorption spectrometry after extraction induced by emulsion breaking. *Microchem J* 153:104401
  52. Mate CJ, Mishra S (2020) Synthesis of borax cross-linked Jhingan gum hydrogel for remediation of Remazol Brilliant Blue R (RBBR) dye from water: adsorption isotherm, kinetic, thermodynamic and biodegradation studies. *Int J Biol Macromol* 151:677–690
  53. Ferrer C, Lozano A, Agüera A, Girón AJ, Fernández-Alba AR (2011) Overcoming matrix effects using the dilution approach in multiresidue methods for fruits and vegetables. *J Chromatogr A* 1218(42):7634–7639. <https://doi.org/10.1016/j.chroma.2011.07.033>
  54. Lefatle MC et al (2023) Preparation, characterization, and application of chitosan–kaolin-based nanocomposite in magnetic solid-phase extraction of tetracycline in aqueous samples. *Chem Pap* 77(3):1601–1618. <https://doi.org/10.1007/s11696-022-02577-3>
  55. Chokwe RC, Dube S, Nindi MM (2020) Development of an HPLC-DAD method for the quantification of ten compounds from *Moringa oleifera* Lam. And its application in Quality Control of Commercial products. *Molecules* 25(19). <https://doi.org/10.3390/molecules25194451>
  56. Lee HB, Sarafin K, Peart TE (2007) Determination of  $\beta$ -blockers and  $\beta_2$ -agonists in sewage by solid-phase extraction and liquid chromatography tandem mass spectrometry. *J Chromatogr A* 1148(2):15
  57. Boonjob W, Sklenářová H, Lara FJ, García-Campaña AM, Solich P (2014) Retention and selectivity of basic drugs on solid-phase extraction sorbents: application to direct determination of  $\beta$ -blockers in urine. *Anal Bioanal Chem* 406:4207–4215
  58. Hemmati M, Asghari A, Bazregar M, Rajabi M (2016) Rapid determination of some beta-blockers in complicated matrices by tandem dispersive liquid-liquid microextraction followed by high performance liquid chromatography. *Anal Bioanal Chem* 408:8163–8176
  59. Salem AA, Wasfi IA, Al-Nassibi SS (2012) Trace determination of  $\beta$ -blockers and  $\beta_2$ -agonists in distilled and waste-waters using liquid chromatography–tandem mass spectrometry and solid-phase extraction. *J Chromatogr B* 908:27–38
  60. Murray GJ, Danaceau JP (2009) Simultaneous extraction and screening of diuretics, beta-blockers, selected stimulants and steroids in human urine by HPLC-MS/MS and UPLC-MS/MS. *J Chromatogr B* 877(30):3857–3864
  61. Serrano M, Chatzimitakos T, Gallego M, Stalikas CD (2016) 1-Butyl-3-aminopropyl imidazolium—functionalized graphene oxide as a nanoadsorbent for the simultaneous extraction of steroids and  $\beta$ -blockers via dispersive solid–phase microextraction. *J Chromatogr A* 1436:9–18
  62. Yıldırım S, Fikarová K, Pilařová V, Nováková L, Solich P, Horstkotte B (2023) Lab-in-syringe automated protein precipitation and salting-out homogenous liquid-liquid extraction coupled online to UHPLC-MS/MS for the determination of beta-blockers in serum. *Anal Chim Acta*, p. 340966

#### Conflict of Interest.

Authors declare no conflict of interest associated with the current study.

**Publisher's Note** Springer Nature remains neutral with regard to jurisdictional claims in published maps and institutional affiliations.